Transition metal impurities as shallow donors in β-Ga_2O_3

Siavash Karbasizadeh,[1] Sai Mu,[1,2] Mark E. Turiansky,[1] and Chris G. Van de Walle[1]

[1] *Materials Department, University of California, Santa Barbara, California 93106-5050, USA*
[2] *Center for Experimental Nanoscale Physics, Department of Physics and Astronomy, University of South Carolina, SC 29208, USA*

(Dated: July 3, 2024)

We present an in-depth investigation of transition-metal impurities (Hf, Zr, Nb and W) as shallow donors in monoclinic Ga_2O_3 using first-principles calculations within the framework of density-functional theory (DFT). A combination of semilocal and hybrid functionals is used to predict their binding energies and hyperfine parameters. The generalized gradient approximation (GGA) allows performing calculations for supercells of up to 2500 atoms, enabling an extrapolation to the dilute limit. The shortcoming of GGA in correctly describing the electron localization is then overcome by the use of the hybrid functional. Results are presented and discussed in light of the application of these transition-metal elements as shallow donors in Ga_2O_3 and their identification in experiment. The methodology applied here can be used in calculations for shallow donors in other systems.

I. INTRODUCTION

Monoclinic Ga_2O_3 (denoted as β-Ga_2O_3) has been attracting a considerable amount of attention over the past few years. This wide-bandgap semiconductor, with a gap of 4.76 eV [1, 2], displays a variety of desirable properties that makes it promising for applications in field effect transistors (FETs) [3, 4], deep ultraviolet photodetectors [5], and Schottky diodes [6]. These properties include a high breakdown field (5-8 MV/cm) [3, 7], ease of n-type doping [8–10], and availability of high-quality bulk crystals [11]. The n-type doping of β-Ga_2O_3 is readily accomplished by introducing shallow donors, in spite of the wide bandgap (comparable to some materials that are considered insulators). β-Ga_2O_3 has two inequivalent Ga sites in its monoclinic structure (see Fig. 1), with octahedral and tetrahedral coordination; impurity incorporation on either site should be considered.

The common shallow donors in β-Ga_2O_3 include silicon, germanium, and tin. Doping of bulk crystals with Si or Sn has been reported to be limited to 2×10^{19} cm^{-3} [12–14] due to formation of a second phase in the case of Si [12] and high evaporation rates in the case of Sn [13, 14]. Doping bulk crystals with Ge has been impeded by the high vapor pressure of Ge [8]. Transition metals have been explored as alternative dopants. Tungsten was reported to incorporate in β-Ga_2O_3 in large concentrations (up to 30.4% W to Ga ratio), without phase transitions to one of the other Ga_2O_3 phases or formation of WO_3 phases [15, 16]. Zirconium was found to be unintentionally incorporated from the insulation used in melt-grown β-Ga_2O_3 and to act as a dopant; it has a low vapor pressure at the melting temperature of β-Ga_2O_3 [17].

Characterization and control of n-type doping requires accurate knowledge of donor binding energies and other properties such as hyperfine parameters. The binding energy determines the electron concentration and is essential for device modeling, while hyperfine parameters are used in identifying and characterizing the donor based on

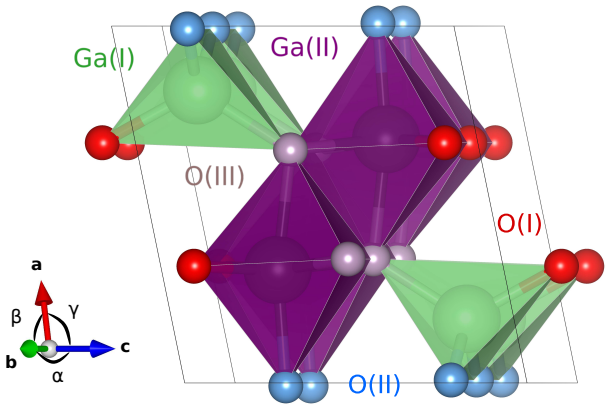

FIG. 1. The 20-atom unit cell of β-Ga_2O_3 that is used as a building block for supercells in this work. The inequivalent Ga and O sites are labeled. Ga(I) (green) and Ga(II) (purple) correspond to tetrahedral and octahedral sites, respectively. For the O sites, threefold coordinated O(I) is depicted in red, threefold coordinated O(II) in blue, and fourfold coordinated O(III) in gray.

electron paramagnetic resonance (EPR) measurements for β-Ga_2O_3[18]. Correctly describing and calculating these quantities is very challenging for shallow donors as their wavefunctions are spread over a very large volume. The binding energy of shallow donors in β-Ga_2O_3 can be estimated from hydrogenic effective mass theory [19], using an effective electron mass of 0.28 m_0 [20] and the dielectric constant of 11.47 [21]. This results in a binding energy of 29 meV and a Bohr radius of 21.3 Å for any shallow donor in Ga_2O_3 regardless of the donor species. More sophisticated semi-empirical approaches can be used, but the dependence on approximations and on input parameters results in a lack of predictive capability. First-principles calculations based on density functional theory (DFT) can in principle provide the required accuracy, but are very challenging due to the extremely large supercells required to capture the extent

of the wavefunction. Recently, Swift *et al.* [22] described a new methodology that allows reaching the dilute limit by extrapolating results obtained for different supercell sizes. The large supercell calculations that are still required are performed using a generalized gradient approximation (GGA) functional, which allows supercell sizes up to 2500 atoms. The shortcoming of GGA in describing localization of the wavefunction is then corrected by performing hybrid functional calculations for select supercells. This approach was found to produce binding energies and hyperfine parameters for As and Bi shallow donors in silicon that are in good agreement with experiment. Here we use the approach of Ref. 22 for transition metal impurities in Ga_2O_3, performing GGA calculations in supercells of up to 2500-atoms and hybrid functional calculations up to 1280 atoms.

A number of transition metal impurities have been explored experimentally and/or computationally as shallow donors in β-Ga_2O_3 [8, 9, 17, 23, 24]. For hafnium (Hf), Saleh *et al.* [8] found from transport measurement that Hf is a shallow donor with high solubility in β-Ga_2O_3 single crystals. They also performed formation energy calculations using a hybrid functional and showed that for Hf incorporation on both tetrahedral (Hf_{tetra}) and octahedral (Hf_{octa}) sites the (+/0) charge-state transition level is within 0.1 eV of the conduction-band minimum (CBM), indicative of a shallow donor. Wu *et al.* [23] also demonstrated n-type conductivity in Hf-doped epitaxial β-Ga_2O_3 thin films fabricated by pulsed laser deposition, and based on Hall measurements they obtained a binding energy of 47.6 meV in heteroepitaxial, and 41.8 meV in homoepitaxial films.

For zirconium (Zr) Saleh *et al.* [17] also reported shallow donor characteristics for Zr-doped β-Ga_2O_3 single crystals with a measured binding energy of $\sim$ 10 meV, and formation-energy calculations with a hybrid functional confirmed the shallow-donor behavior for Zr in both tetrahedral and octahedral coordination.

Niobium (Nb) is a potential double donor. Zhou *et al.* [24] found Nb to be an effective n-type dopant for β-Ga_2O_3. DFT calculations with a hybrid functional [9] also found shallow-donor character and reported very low formation energies.

Tungsten (W), finally, has not yet been explored experimentally, but based on calculations of formation energies [9] W_{tetra} was found to act as a shallow donor with a modest formation energy. W_{octa}, on the other hand, was found to act as a deep donor, with a (+/0) transition level 0.58 eV below the CBM.

This paper is organized as follows: Sec. II provides the details of the first-principles calculations and methodology. Section III discusses the main results of the study. Binding energies are presented in Sec. III A, and isotropic hyperfine parameters are reported in Sec. III B. Section IV concludes the paper.

TABLE I. Calculated and experimental [33, 34] lattice parameters for the 20-atom conventional cell of β-Ga_2O_3.

	Calc. (GGA)	Calc. (HSE)	Exp.
a (Å)	12.46	12.24	12.21
b (Å)	3.09	3.04	3.04
c (Å)	5.91	5.80	5.80
β	103.74°	103.82°	103.83°

II. COMPUTATIONAL METHODOLOGY

We perform first-principles calculations based on DFT and the projector augmented wave (PAW) method [25] as implemented in the Vienna *ab-initio* simulation package (VASP) [26, 27]. The PAW pseudopotentials have the valence electron configurations of $4s^2 4p^1$ for Ga and $2s^2 2p^4$ for O, and $5s^2 5p^6 6s^2 5d^2$ for Hf, $4s^2 4p^6 5s^2 4d^2$ for Zr, $4s^2 4p^6 5s^1 4d^4$ for Nb and $5s^2 5p^6 6s^2 5d^4$ for W. Tests showed that inclusion of Ga d states as valence states did not affect the results. We employ the GGA exchange correlation functional of Perdew, Burke and Ernzerhof (PBE) [28] for the very large supercell calculations used for extrapolation, and the hybrid functional of Heyd, Scuseria and Ernzerhof (HSE) [29] for select supercells to provide a proper description of wavefunction localization. The mixing parameter in HSE is set to α=0.32, yielding a bandgap of 4.9 eV for β-Ga_2O_3 [30]. In cases where GGA is inadequate to properly account for the localization of d orbitals, we use the spherically averaged DFT+U method [31] to describe the Coulomb correlations within the d shells, with Coulomb correlation parameters U = 3 eV for Nb and 4 eV for W. The U values were chosen to best reproduce the results in the HSE calculations, the criteria being obtaining a high-spin state and the presence of localized Kohn-Sham states deep in the band gap (see Sec. III A 3). In practice, we gradually increased the value of U, in 160-atom and 540-atom supercells until these criteria were met. Increasing U further did not have any notable effect on the calculated properties and therefore we did not engage in fine-tuning U. Spin polarization is included in all calculations. A kinetic energy cutoff of 450 eV for plane-wave expansion is employed.

Supercells for calculating properties of impurities are constructed by taking a multiple of the unit cell of the material. The primitive cell of β-Ga_2O_3 contains 10 atoms, but often a 20-atom conventional cell is used [32]. Lattice parameters of the conventional cell are given in Table I for both GGA and HSE functionals. We can see good agreement with experimental values [33, 34]. Neither of these cells is a good choice for constructing supercells, since they do not lead to comparable separation between impurities in all three spatial directions. To address this issue we adopted a different unit cell (Fig. 1) that contains 20 atoms and has nearly equal-length lattice parameters (a, b, c) and angles α, β and γ that are close to 90°.

The following transformation connects the lattice vectors $\mathbf{a}'$, $\mathbf{b}'$, $\mathbf{c}'$ of this cell to the lattice vectors $\mathbf{a}$, $\mathbf{b}$, $\mathbf{c}$ of the 10-atom primitive cell:

$$\begin{pmatrix}\mathbf{a}'\\ \mathbf{b}'\\ \mathbf{c}'\end{pmatrix} = \begin{pmatrix}0 & 1 & 0\\ 2 & 2 & 0\\ 0 & 0 & 1\end{pmatrix}\begin{pmatrix}\mathbf{a}\\ \mathbf{b}\\ \mathbf{c}\end{pmatrix}. \quad (1)$$

$n \times n \times n$ supercells based on this 20-atom cell provide nearly uniform separation between the impurity and its periodic images along the three cartesian directions. The smallest supercell (n=2) contains N=20×$n \times n \times n$=160 atoms. For GGA calculations, we can go up to n=5, which results in a 2500-atom supercell. For the more computationally demanding HSE functional, n=4 (1280 atoms) is the largest achievable. To fill the gap between the n=3 cell with 540 atoms and the n=4 cell with 1280 atoms we also used a 2×6×4 multiple of the 20-atom conventional cell [32]. This cell contains 960 atoms and will be denoted as 960_{conv}.

The Brillouin-zone is sampled using a Γ-centered k-point grid of 8×8×8 for the unit cell. Calculations for supercells are performed with a single k-point at Γ. Tests indicated that this is adequate for supercells with $n \geq 3$; we will see later that n=2 (160-atom) supercells are too small to obtain accurate values, anyway.

Atomic relaxations in the 20-atom unit cell are performed until the Hellmann-Feynman forces on each atom are less than 5 meV/Å, while for the supercell calculations, the force convergence criterion is set to 10 meV/Å. To make the atomic relaxation of larger supercells more computationally affordable, an embedding technique is used: the relaxed atomic positions obtained for an $(n \times n \times n)$ supercell are used as initial positions for the atoms around the impurity within a larger $((n+1) \times (n+1) \times (n+1))$ supercell. For the HSE calculations, where performing atomic relaxations in large supercells is particularly expensive, we additionally take advantage of the knowledge of atomic positions for atoms not included in the $(n \times n \times n)$ supercell as obtained in PBE calculations of the same supercell (taking appropriate scaling of the lattice parameters into account). These procedures speed up the atomic relaxation of the supercells considerably and thus reduce the computational cost.

The binding energy of a shallow donor is calculated as [22]:

$$E_b = \epsilon_\Gamma^{\text{CB}} - \epsilon_\Gamma^{\text{donor}} + e\Delta V. \quad (2)$$

$\epsilon_\Gamma^{\text{CB}}$ is the Kohn-Sham eigenvalue of the CBM in a bulk calculation, and $\epsilon_\Gamma^{\text{donor}}$ is the Kohn-Sham eigenvalue of the occupied donor state, both calculated at the Γ point in a supercell of a given size. These eigenvalues are referenced to the average electrostatic potential, which shifts when an impurity is added to the supercell. The last term in the equation, $e\Delta V$, accounts for aligning the eigenvalues in the supercell containing the impurity with the eigenvalues in the bulk and impurity related calculations. We obtain $\Delta V = \langle V^{\text{bulk}} - V^{\text{donor}} \rangle$ by performing a macroscopic average over a bulk-like region of the cell far from the donor.

The isotropic hyperfine parameter (in SI units) is given by:

$$A = \frac{2\mu_0}{3} g_e \mu_B g_I \mu_N \int \delta_T(r-R)\sigma(r)dr, \quad (3)$$

where g_e is the electron g-factor, μ_B is the Bohr magneton, g_I is the g-factor of the nucleus of the dopant, μ_N is the nuclear magneton, R is the position of the nucleus, and $\sigma(r)$ is the spin density. Calculations are performed following the methodology outlined in Refs. 35–38. The frozen valence approximation (developed in Ref. [38] and validated in the context of HSE in Ref. [35]) is used, and core spin polarization is taken into account.

III. RESULTS AND DISCUSSION

A. Binding Energy

1. *Hafnium*

DFT calculations with a hybrid functional [8] previously produced formation energies (under Ga-rich conditions and with the Fermi level at the CBM) of 1.49 eV for Hf_{octa} and 2.65 eV for Hf_{tetra}. In thermodynamic equilibrium Hf_{octa} is therefore expected to be more dominant. However, since dopant incorporation may be subject to kinetic limitations during growth, or could be performed by ion implantation, we calculate the properties of Hf on both tetrahedral and octahedral sites.

Hf donates a single electron to the system. The effects of spin polarization are manifested in the splitting observed for the eigenvalue of the donor state: the exchange splitting is defined as the eigenvalue difference between the occupied and unoccupied donor states in spin-polarized (SP) calculations. We checked that the lowering of $\epsilon_\Gamma^{\text{donor}}$ when compared to the non-spin-polarized (NSP) value corresponds to half of the exchange splitting: $\delta\epsilon_\Gamma^{\text{donor}} = \epsilon_{\Gamma,\text{NSP}}^{\text{donor}} - \epsilon_{\Gamma,\text{SP}}^{\text{donor}}$. The exchange splitting is supercell-size dependent and scales linearly with the inverse of the supercell volume (or inverse of number of atoms in the supercell), as shown in Fig. 2 for both GGA and HSE, based on values listed in Table II.

We also found that spin polarization does not affect the alignment term in Eq. (2). These results show that for purposes of extrapolating results as a function of supercell size, the effect of exchange splitting on the binding energy (and, specifically, the difference between GGA and HSE) can be accurately taken into account using linear fits based on relatively small supercells.

The other values needed to obtain the binding energy of the Hf dopant [Eq. (2)] are also shown in Table II. The resulting values for SP binding energies calculated using GGA and HSE are then plotted in Fig. 3. For GGA, we note that 160-atom supercells are too small for extracting

TABLE II. Calculated parameters for Hf shallow donors: Kohn-Sham eigenvalues $\epsilon_\Gamma^{\rm CB}$ and $\epsilon_\Gamma^{\rm donor}$ (eV) (SP), electrostatic potential alignment (meV), and the resulting binding energies (meV) (SP) for different supercell sizes, computed with GGA and HSE functionals.

		bulk		Hf_{tetra}			Hf_{octa}	
N	n	$\epsilon_\Gamma^{\rm CB}$	$e\Delta V$	$\epsilon_{\Gamma,\rm SP}^{\rm donor}$	$E_{b,\rm SP}$	$e\Delta V$	$\epsilon_{\Gamma,\rm SP}^{\rm donor}$	$E_{b,\rm SP}$
				GGA				
160	2	3.3670	104.0	3.4527	18.3	91.0	3.4630	-5.0
540	3	3.3625	48.0	3.3877	26.2	47.0	3.3906	18.9
960	-	3.3623	37.6	3.3756	24.3	35.6	3.3773	20.6
1280	4	3.3622	32.3	3.3720	22.5	31.0	3.3732	20.0
2500	5	3.3622	23.0	3.3661	19.1	23.6	3.3667	19.1
				HSE				
160	2	4.9191	113.6	4.7855	247.2	99.6	4.7990	219.7
540	3	4.9017	52.0	4.8599	93.8	52.6	4.8637	90.6
960	-	4.9007	42.6	4.8751	68.2	41.0	4.8774	64.3
1280	4	4.9005	36.0	4.8808	55.7	35.3	4.8824	53.4

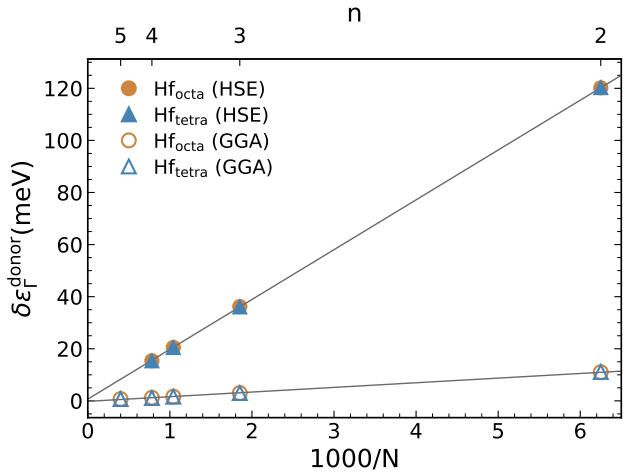

FIG. 2. Half of the exchange splitting $\delta\epsilon_\Gamma^{\rm donor}$ (in meV) as a function of the inverse of the supercell size for Hf_{tetra} and Hf_{octa} in β-Ga_2O_3, as obtained from GGA and HSE calculations. The values for Hf_{tetra} and Hf_{octa} are nearly identical, and linear scaling is seen in all cases. Linear fits result in $\delta\epsilon_\Gamma^{\rm donor}$(GGA) = -0.2 + 1.78 $\times$ 1000/N and $\delta\epsilon_\Gamma^{\rm donor}$(HSE) = 0.7 + 19.13 $\times$ 1000/N.

a meaningful binding energy, and the accuracy of the fit is also improved by excluding the N=540 data point. By omitting these two data points, N=160 and N=540, we obtain a good fit to the $1/N$ dependence. For Hf_{tetra}, the extrapolation to the dilute limit of the linear fit in Fig. 3(a) yields a binding energy of 15.9 meV.

To correct for an underestimation of localization in the GGA functional, we perform HSE calculations, for which the largest achievable supercell is N=1280. Assuming that the supercell-size dependence of E_b is similar in GGA and HSE, we then fit the linear extrapolation obtained from GGA through the HSE N=1280 data point, but adjust the slope to take the difference in (half) the exchange splitting into account. From Fig. 2 half of the exchange splitting amounts to (in meV) $\delta\epsilon_\Gamma^{\rm donor}$(HSE)-$\delta\epsilon_\Gamma^{\rm donor}$(GGA) = 0.8 + 17.35 $\times$ 1000/N. The resulting value (see the caption of Fig. 2 for the equations) leads to a binding energy of 35.8 meV for Hf_{tetra} in HSE. Applying the same procedure to Hf_{octa} [Fig. 2(b)] leads to a binding energy of 18.2 meV in GGA and 38.0 meV in HSE. We note that the binding energy is not very sensitive to the site (tetrahedral or octahedral) on which the impurity is incorporated. Our HSE values are in satisfactory agreement with the activation energy of 41.8 meV reported by Wu *et al.* [23] based on the temperature dependence of resistance of Hf-doped homoepitaxial films.

2. *Zirconium*

We now apply the same procedure to the other transition metal impurities. Because of the qualitative similarity to the results for Hf, we include the results for other impurities in Supporting Information.

Table S1, Supporting Information, contains the calculated parameters for Zr, which is also a single donor. Data for exchange splitting are shown in Fig. S1, Supporting Information; the values are very similar to those for Hf. Binding energies are shown in Fig. S2, Supporting Information, for both tetrahedral and octahedral coordination using GGA and HSE functionals. The resulting HSE binding energies are 35.1 meV for Zr_{tetra} and 35.5 meV for Zr_{octa}. These values are similar to those obtained for Hf. Saleh *et al.* reported a value as low as $\sim$10 meV for the activation energy of the carrier concentration extracted from temperature-dependent Hall measurements. We note that such an activation energy does not necessarily correspond to the binding energy of the donor.

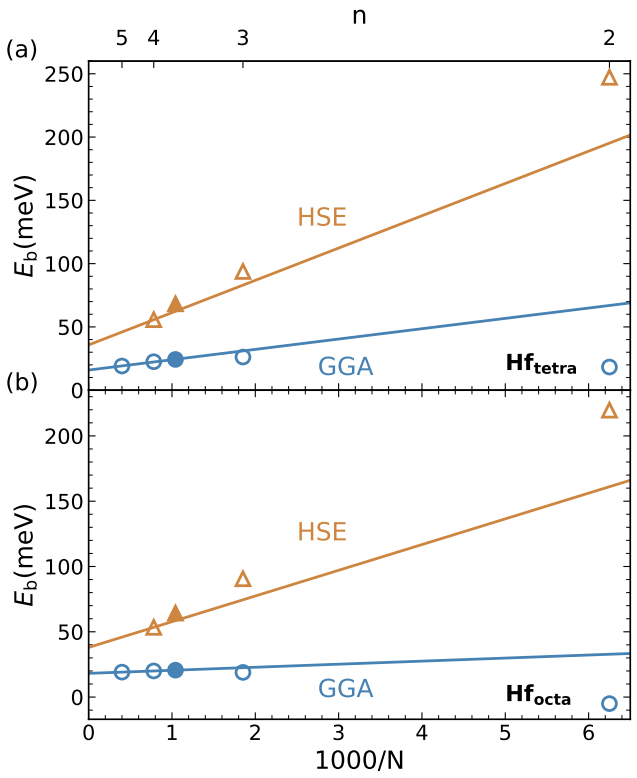

FIG. 3. Binding energies for (a) Hf_{tetra} and (b) Hf_{octa} donors as a function of supercell size, based on SP calculations. GGA data points are denoted by blue circles and HSE data points by orange triangles. The filled markers represent the 960-atom supercell. The blue lines are linear fits to GGA data for $N \geq 960$; the orange lines use the same extrapolation as the GGA data but account for the difference in exchange splitting between GGA and HSE and pass through the $N = 1280$ HSE data point. The fits correspond to, for Hf_{tetra}: $E_{b,\mathrm{SP}}(\mathrm{GGA}) = 15.9 + 8.16 \times 1000/N$ and $E_{b,\mathrm{SP}}(\mathrm{HSE}) = 35.8 + 25.51 \times 1000/N$; and for Hf_{octa}: $E_{b,\mathrm{SP}}(\mathrm{GGA}) = 18.2 + 2.34 \times 1000/N$ and $E_{b,\mathrm{SP}}(\mathrm{HSE}) = 38.0 + 19.69 \times 1000/N$.

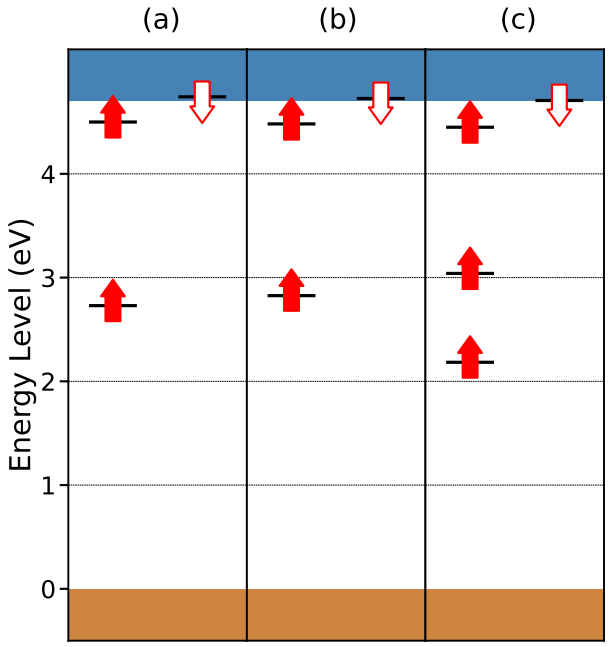

FIG. 4. Occupation of Kohn-Sham states in the band gap for (a) Nb_{tetra}, (b) Nb_{octa} and (c) W_{tetra} in β-Ga_2O_3, calculated using HSE in the 160-atom supercell.

3. *Niobium*

Contrary to Hf and Zr, which act as single donors, Nb is a double donor. Spin-polarized calculations with HSE reveal that the total spin in the ground state of the Nb donor is equal to 1, i.e., the two electrons go into the same spin channel. Figs. 4(a) and (b) show the occupation of impurity-induced Kohn-Sham states in the band gap for Nb_{tetra} and Nb_{octa}, obtained from SP HSE calculations in a 160-atom supercell. The energy difference between the high (S=1) and low ($S = 0$) spin states is 559 meV for Nb_{tetra} and 1 meV for Nb_{octa}. Fig. 4 shows that both Nb_{tetra} and Nb_{octa} have a deep-lying Kohn-Sham state, in addition to the shallow states near the CBM. The GGA functional is incapable of correctly describing this state, and incorrectly predicts the S=0 state to be the ground state, a well-known problem when calculating transition-metal impurities with a semilocal functional. We apply a well-established fix to this, namely to include a Coulomb correlation correction U to the d orbitals of Nb. A U value of 3 eV ensures that the high-spin state is stabilized.

Binding-energy calculations for Nb are then performed using GGA+U and HSE functionals. Table S2, Supporting Information, contains the calculated parameters. Data for exchange splitting are shown in Fig. S3, Supporting Information; note that the values are again very similar to those for Hf and Zr. Binding energies are shown in Fig. S4, Supporting Information, for both tetrahedral and octahedral coordination using GGA+U and HSE functionals. The resulting HSE binding energies are 36.9 meV for Nb_{tetra} and 36.3 meV for Nb_{octa}, again very similar for both sites, and similar to the values obtained for Hf and Zr.

4. *Tungsten*

As noted in Sec. I, W_{octa} was shown not to be a shallow donor [9], therefore we focus on W_{tetra} in our study of binding energies. Using HSE, the triple donor W_{tetra} again has the high spin state as the ground state, 177 meV lower in energy than the low spin state. In the high spin state, three electrons reside in the spin-up channel [Fig. 4(c)], giving a net magnetization of 3 μ_B; two electrons are in Kohn-Sham states deep within the gap while one electron is in a state close to the CBM. We again need to apply GGA+U to obtain the correct ground state, with a U value of 4 eV. Parameters required for calcu-

lating the binding energy of W_{tetra} are listed in Table S3, Supporting Information, and fitting of the exchange splitting is shown in Fig. S5, Supporting Information. Binding energies are shown in Fig. S6, Supporting Information. The resulting HSE binding energy for W_{tetra} is 36.1 meV, again very similar to the values obtained for the other transition-metal impurities.

A summary of the binding energies for the investigated transition metals is given in Table III.

B. Hyperfine Parameters

For calculating hyperfine parameters, we choose an isotope that is stable and carries a nuclear spin. For the Hf donor, we select ^{177}Hf; the results for the isotropic hyperfine parameters of ^{177}Hf [Eq. 3] are shown in Fig. 5. An extrapolation procedure similar to that for binding energies is followed: we apply linear fitting to GGA values for $N \geq 960$ data points. Extrapolation gives $A(\mathrm{GGA}) = -0.8$ MHz for Hf_{tetra} and -0.8 MHz for Hf_{octa}. To calculate the hyperfine parameter in HSE, the GGA-fitted line is shifted without changing its slope. In the case of binding energies the slope adjustment reflects the difference in exchange splitting between PBE and HSE; for hyperfine parameters, no such adjustment is needed. Instead of shifting the line to pass through the HSE data point for the largest supercell, the intercept is adjusted to optimally fit to the data points for the largest three supercells (with $N \geq 540$). HSE values for hyperfine parameters converge faster than HSE binding energies, and therefore folding in information from the largest three supercells is appropriate. We note, however, that using only the HSE data point for the largest supercell would not significantly change our results. This leads to $A(\mathrm{HSE})=-1.8$ MHz for Hf_{tetra} and -2.7 MHz for Hf_{octa}.

Fig. S7, Supporting Information, shows hyperfine parameters calculated for the ^{91}Zr donor. Following a similar procedure, we obtain extrapolated HSE values of -1.5 for Zr_{tetra} and 0.8 MHz for Zr_{octa}. Fig. S8, Supporting Information, shows hyperfine parameters calculated for the ^{93}Nb donor, presenting GGA+U and HSE values. The extrapolation procedure yields HSE values of -126.4 MHz for Nb_{tetra} and -50.2 MHz for Nb_{octa}. For W_{tetra} (^{183}W), finally, we obtain -32.6 MHz (Fig. S9, Supporting Information). Dipolar contributions to the hyperfine structure for Nb and W, unlike Hf and Zr, are not negligible and hence are reported in Tables S4-6, Supporting Information.

The calculated isotropic hyperfine parameters are summarized in Table III.

IV. CONCLUSION

We studied the transition metals Hf, Zr, Nb, and W as shallow dopants in β-Ga_2O_3. Binding energies and hyperfine parameters were calculated for each shallow donor using a predictive first-principles model. Our results show that the binding energies for the various impurities are comparable, and close to those of Si and Ge [39, 40]. These energies deviate by only a small amount from the binding energy of 29 meV predicted by hydrogenic effective mass theory. Our predictions of hyperfine parameters should aid experimental identification.

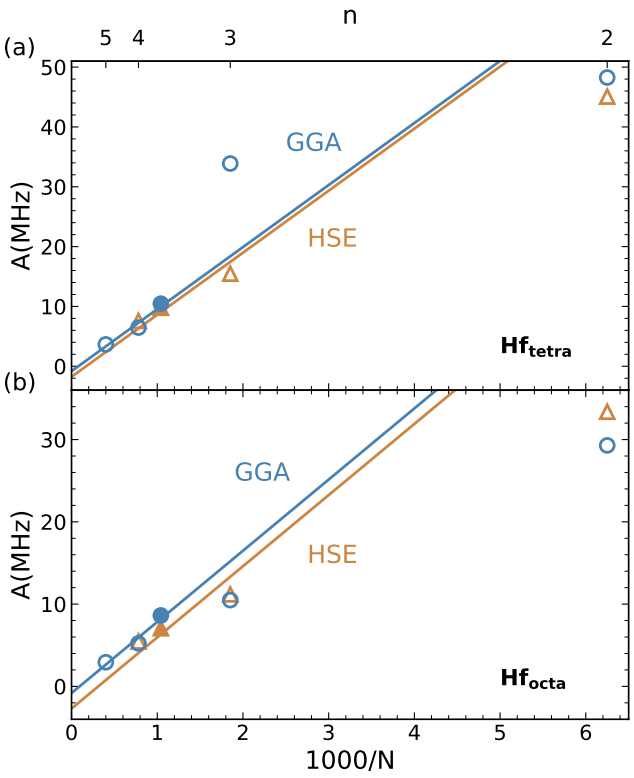

FIG. 5. Isotropic hyperfine parameters for (a) Hf_{tetra} and (b) Hf_{octa} donors as a function of supercell size. GGA data points are in blue circles and HSE data points are in orange triangles. The filled markers represent the 960-atom supercell. The blue lines are linear fits to GGA data for $N \geq 960$; the orange lines are rigid shifts of the blue lines, intercept fits to the HSE data for $N \geq 540$. The fits correspond to, for Hf_{tetra}: $A(\mathrm{GGA}) = -0.8 + 10.37 \times 1000/N$ and $A(\mathrm{HSE}) = -1.8$ MHz $+ 10.37 \times 1000/N$; and for Hf_{octa}: $A(\mathrm{GGA}) = -0.8 + 8.65 \times 1000/N$ and $A(\mathrm{HSE}) = -2.7 + 8.65 \times 1000/N$.

V. SUPPORTING INFORMATION

Supporting information is available from the Wiley Online Library or from the author.

VI. ACKNOWLEDGMENTS

This work is supported by the GAME MURI of the Air Force Office of Scientific Research (FA9550-18-1-0479). We used computational facilities purchased with funds

TABLE III. Summary of calculated isotropic hyperfine parameters (MHz) for ^{177}Hf, ^{91}Zr, ^{93}Nb, and ^{183}W. Calculated binding energies (meV) are also listed.

	Hf_{tetra}	Hf_{octa}	Zr_{tetra}	Zr_{octa}	Nb_{tetra}	Nb_{octa}	W_{tetra}
Hyperfine parameter	−1.8	−2.7	−1.5	0.8	−126.4	−50.2	−32.6
Binding energy	35.8	38.0	35.1	35.5	36.9	36.3	36.1

from the National Science Foundation (NSF) (CNS-1725797) and administered by the Center for Scientific Computing (CSC). The CSC is supported by the California NanoSystems Institute and the Materials Research Science and Engineering Center (MRSEC; NSF DMR 1720256) at the University of California Santa Barbara. We also used computing resources through allocation DMR070069 provided by the Advanced Cyberinfrastructure Coordination Ecosystem: Services and Support (ACCESS), supported by NSF Grant numbers 2138259, 2138286, 2138307, 2137603, and 2138296.

VII. CONFLICT OF INTEREST

The authors declare no conflict of interest.

VIII. DATA AVAILABILITY STATEMENT

The data that support the findings of this study are available from the corresponding author upon reasonable request.

[1] H. H. Tippins, Phys. Rev. **140**, A316 (1965).
[2] T. Matsumoto, M. Aoki, A. Kinoshita, and T. Aono, Jpn. J. Appl. Phys. **13**, 1578 (1974).
[3] M. Higashiwaki, K. Sasaki, A. Kuramata, T. Masui, and S. Yamakoshi, Appl. Phys. Lett. **100**, 013504 (2012).
[4] W. S. Hwang, A. Verma, H. Peelaers, V. Protasenko, S. Rouvimov, H. (Grace) Xing, A. Seabaugh, W. Haensch, C. G. Van de Walle, Z. Galazka, M. Albrecht, R. Fornari, and D. Jena, Appl. Phys. Lett. **104**, 203111 (2014).
[5] T. Oshima, T. Okuno, and S. Fujita, Jpn. J. Appl. Phys. **46**, 7217 (2007).
[6] K. Konishi, K. Goto, H. Murakami, Y. Kumagai, A. Kuramata, S. Yamakoshi, and M. Higashiwaki, Appl. Phys. Lett. **110**, 103506 (2017).
[7] Z. Xia, H. Chandrasekar, W. Moore, C. Wang, A. J. Lee, J. McGlone, N. K. Kalarickal, A. Arehart, S. Ringel, F. Yang, and S. Rajan, Appl. Phys. Lett. **115**, 252104 (2019).
[8] M. Saleh, J. B. Varley, J. Jesenovec, A. Bhattacharyya, S. Krishnamoorthy, S. Swain, and K. Lynn, Semicond. Sci. Technol. **35**, 04LT01 (2020).
[9] H. Peelaers and C. G. Van de Walle, Phys. Rev. B **94**, 195203 (2016).
[10] J. B. Varley, J. R. Weber, A. Janotti, and C. G. Van de Walle, Appl. Phys. Lett. **97**, 142106 (2010).
[11] E. G. Víllora, K. Shimamura, Y. Yoshikawa, K. Aoki, and N. Ichinose, J. Crys. Growth **270**, 420 (2004).
[12] E. G. Víllora, K. Shimamura, Y. Yoshikawa, T. Ujiie, and K. Aoki, Appl. Phys. Lett. **92**, 202120 (2008).
[13] Z. Galazka, K. Irmscher, R. Uecker, R. Bertram, M. Pietsch, A. Kwasniewski, M. Naumann, T. Schulz, R. Schewski, D. Klimm, and M. Bickermann, J. Cryst. Growth **404**, 184 (2014).
[14] A. Kuramata, K. Koshi, S. Watanabe, Y. Yamaoka, T. Masui, and S. Yamakoshi, Jpn. J. Appl. Phys. **55**, 1202A2 (2016).
[15] A. A. Dakhel, J. Mater. Sci. **47**, 3034 (2012).
[16] E. J. Rubio and C. V. Ramana, Appl. Phys. Lett. **102**, 191913 (2013).
[17] M. Saleh, A. Bhattacharyya, J. B. Varley, S. Swain, J. Jesenovec, S. Krishnamoorthy, and K. Lynn, Appl. Phys. Express **12**, 085502 (2019).
[18] B. Meyer, U. Leib, A. Hofstätter, C. Krummel, and D. Kohl, in *Defects in Semiconductors 19*, Materials Science Forum, Vol. 258 (Trans Tech Publications Ltd, 1997) pp. 1473–1478.
[19] P. Y. Yu and M. Cardona, in *Fundamentals of Semiconductors*, Graduate Texts in Physics (Springer, Berlin, 2010).
[20] M. Mohamed, C. Janowitz, I. Unger, R. Manzke, Z. Galazka, R. Uecker, R. Fornari, J. R. Weber, J. B. Varley, and C. G. Van de Walle, Appl. Phys. Lett. **97**, 211903 (2010).
[21] M. Schubert, R. Korlacki, S. Knight, T. Hofmann, S. Schöche, V. Darakchieva, E. Janzén, B. Monemar, D. Gogova, Q.-T. Thieu, R. Togashi, H. Murakami, Y. Kumagai, K. Goto, A. Kuramata, S. Yamakoshi, and M. Higashiwaki, Phys. Rev. B **93**, 125209 (2016).
[22] M. W. Swift, H. Peelaers, S. Mu, J. J. L. Morton, and C. G. Van de Walle, npj Comput. Mater. **6**, 181 (2020).
[23] S. Wu, N. Liu, H. Li, J. Zhang, S. Shen, W. Wang, N. Xia, Y. Cao, Z. Zhong, W. Zhang, and J. Ye, Phys. Status Solidi RRL , 2300110 (2023).
[24] W. Zhou, C. Xia, Q. Sai, and H. Zhang, Appl. Phys. Lett. **111**, 242103 (2017).
[25] P. E. Blöchl, Phys. Rev. B **50**, 17953 (1994).
[26] G. Kresse and J. Hafner, Phys. Rev. B **48**, 13115 (1993).
[27] G. Kresse and J. Furthmüller, Phys. Rev. B **54**, 11169 (1996).
[28] J. P. Perdew, K. Burke, and M. Ernzerhof, Phys. Rev. Lett. **77**, 3865 (1996).
[29] J. Heyd, G. E. Scuseria, and M. Ernzerhof, J. Chem. Phys. **118**, 8207 (2003).
[30] H. Peelaers, J. B. Varley, J. S. Speck, and C. G. Van de Walle, Appl. Phys. Lett. **112**, 242101 (2018).

[31] S. L. Dudarev, G. A. Botton, S. Y. Savrasov, C. J. Humphreys, and A. P. Sutton, Phys. Rev. B **57**, 1505 (1998).
[32] H. Peelaers and C. G. Van de Walle, Phys. Status Solidi B **252**, 828 (2015).
[33] S. Geller, J. Chem. Phys. **33**, 676 (2004).
[34] J. Åhman, G. Svensson, and J. Albertsson, Acta Crystallogr. C **52**, 1336 (1996).
[35] K. Szász, T. Hornos, M. Marsman, and A. Gali, Phys. Rev. B **88**, 075202 (2013).
[36] P. E. Blöchl, Phys. Rev. B **62**, 6158 (2000).
[37] C. G. Van de Walle and P. E. Blöchl, Phys. Rev. B **47**, 4244 (1993).
[38] O. V. Yazyev, I. Tavernelli, L. Helm, and U. Röthlisberger, Phys. Rev. B **71**, 115110 (2005).
[39] Z. Feng, A. F. M. Anhar Uddin Bhuiyan, M. R. Karim, and H. Zhao, Appl. Phys. Lett. **114**, 250601 (2019).
[40] A. T. Neal, S. Mou, S. Rafique, H. Zhao, E. Ahmadi, J. S. Speck, K. T. Stevens, J. D. Blevins, D. B. Thomson, N. Moser, K. D. Chabak, and G. H. Jessen, Appl. Phys. Lett. **113**, 062101 (2018).